

# Turbidity suppression from the ballistic to the diffusive regime in biological tissues using optical phase conjugation

## Emily J. McDowell

California Institute of Technology  
Department of Bioengineering  
1200 East California Boulevard  
Mail Code 136-93  
Pasadena, California 91125

## Meng Cui

California Institute of Technology  
Department of Electrical Engineering  
1200 East California Boulevard  
Mail Code 136-93  
Pasadena, California 91125

## Ivo M. Vellekoop

University of Zurich  
Physics Institute  
Winterthurerstrasse 190  
8257 Zurich, Switzerland

## Vahan Senekerimyan

### Zahid Yaqoob\*

California Institute of Technology  
Department of Electrical Engineering  
1200 East California Boulevard  
Mail Code 136-93  
Pasadena, California 91125

## Changhui Yang

California Institute of Technology  
Department of Bioengineering  
and  
Department of Electrical Engineering  
1200 East California Boulevard  
Mail Code 136-93  
Pasadena, California 91125

## 1 Introduction

Elastic light scattering can significantly confound structural and functional information when biological samples are probed with light. Our recently published experimental technique utilizing optical phase conjugation<sup>1</sup> (OPC) has shown promise in dealing with the problem of light scattering. This method, termed turbidity suppression through optical phase conjugation (TSOPC), employs static holography to force a scattered light field to retrace its path through a highly scat-

**Abstract.** We describe the amplitude and resolution trends of the signals acquired by turbidity suppression through optical phase conjugation (TSOPC) with samples that span the ballistic and diffusive scattering regimes. In these experiments, the light field scattered through a turbid material is written into a hologram, and a time-reversed copy of the light field is played back through the sample. In this manner, the wavefront originally incident on the sample is reconstructed. We examine a range of scattering samples including chicken breast tissue sections of increasing thickness and polyacrylamide tissue-mimicking phantoms with increasing scattering coefficients. Our results indicate that only a small portion of the scattered wavefront ( $<0.02\%$ ) must be collected to reconstruct a TSOPC signal. Provided the sample is highly scattering, all essential angular information is contained within such small portions of the scattered wavefront due to randomization by scattering. A model is fitted to our results, describing the dependence of the TSOPC signal on other measurable values within the system and shedding light on the efficiency of the phase conjugation process. Our results describe the highest level of scattering that has been phase conjugated in biological tissues to date. © 2010 Society of Photo-Optical Instrumentation Engineers. [DOI: 10.1117/1.3381188]

Keywords: optical phase conjugation; light scattering; tissue optics.

Paper 09539R received Dec. 3, 2009; revised manuscript received Feb. 16, 2010; accepted for publication Feb. 19, 2010; published online Apr. 29, 2010.

tering medium, effectively “time reversing” the light scattering process. In this paper, we investigate both the fraction and shape of the light field reconstructed through a variety of samples, including those with the highest level of scattering “time reversed” to date using TSOPC on tissue samples. These samples exhibit scattering that spans both the ballistic and diffusive regimes, which is examined both experimentally and theoretically in terms of amplitude.

Although the applications to biological tissues are new, it was shown over 40 yr ago that OPC could reverse light scattering through a ground glass slide.<sup>2</sup> Phase conjugation has also proven to be useful for removing aberrations associated with optical components for high-resolution imaging<sup>3</sup> and for the optimization of laser cavities.<sup>4,5</sup>

Address all correspondence to: Emily J. McDowell, California Institute of Technology, Department of Bioengineering, 1200 East California Boulevard, Mail Code 136-93, Pasadena, California 91125. Tel: 626-395-2449; Fax: 626-395-8475; E-mail: emilymcd@caltech.edu.

\*Current address: Massachusetts Institute of Technology, G. R. Harrison Spectroscopy Laboratory, 77 Massachusetts Avenue, 6-205, Cambridge, Massachusetts 02139.

Our work employs both sections of chicken breast tissue of varying thickness and tissues phantoms of varying scattering coefficients to analyze the TSOPC process as the level of scattering is increased. We then fit these results to a theoretical model in which the contributions of ballistic and diffuse components are tracked. In doing so we uncover several interesting facts. First, we show that the TSOPC signal amplitude falls off at a slower rate compared to the ballistic (or unscattered) light component, which is inferred to be relatively insignificant in TSOPC signal generation. We also show that reconstruction of the incident wavefront can be performed using only a very small fraction of the scattered light field (as little as 0.02%), provided the sample is highly scattering. Finally, we discuss the nonintuitive finding that the quality of the reconstruction improves as the level of scattering increases, implying that for the most highly scattering samples we examined, a complete subset of information required for reconstruction is included in the 0.02% of the scattered light that is collected.

We will briefly discuss where TSOPC falls in the context of standard optical methods that deal with the challenge of light scattering. Many techniques that acquire depth-resolved information from tissues, such as optical coherence tomography<sup>6</sup> (OCT), selectively gate out and process only “information-bearing” ballistic or singly scattered components through coherent detection mechanisms. Alternatively, diffuse optical methods gather information from multiply scattered, or diffuse, photons exiting a biological material.<sup>7,8</sup> This leads to an increase in penetration depth, but a reduction in resolution.<sup>7</sup> Techniques such as OCT exploit the wave nature of light, while diffuse optical methods model the photons as particles that diffuse through tissue. Our TSOPC technique falls at a junction of these fields, attempting to extract coherent information from the bulk of the multiply scattered light. Here, we show a TSOPC signal, dependent on coherent detection and playback mechanisms, for light fields that have experienced over 200 scattering events.

Our specific methods involve two main steps: (1) collection and (2) “time reversal” of scattered light components. Note that the phrase “time reversal” is intended to help the reader envision the experiment. This process is not a true time reversal for two reasons. First, the collection area is of finite size, and the uncollected information is missing from playback. Second, even if the collection area was very large, collection in the far field means that the evanescent component of the scattered light field cannot be collected, and is missing as well. Current research efforts in which a shaped input beam is used to optimize transmission through a scattering medium<sup>9,10</sup> are complementary to the second step of our process.

In this manuscript, we (1) describe our TSOPC setup, (2) determine the TSOPC signal amplitude trend for an increasing average number of scattering events in both tissue and tissue-mimicking phantoms with varying angular scattering properties, (3) examine the TSOPC resolution as the level of scattering increases, and (4) model and discuss the origin of the amplitude trend based on other measurable signals in our system.

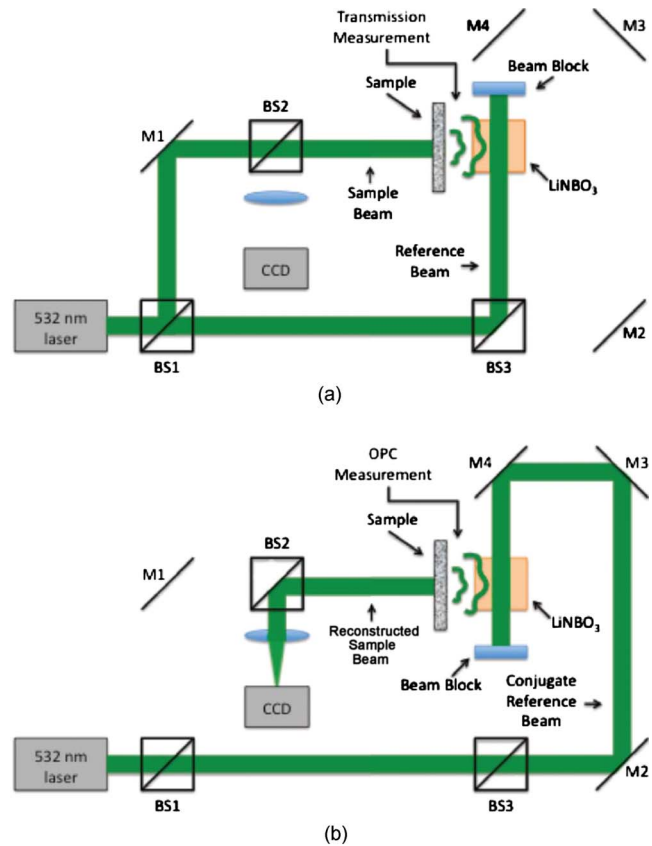


**Fig. 1** (a) System setup for the recording process. Light scattered on transmission through a sample interfered with a reference beam in a photorefractive crystal (PrC) over tens of seconds. A transmission measurement was made at the location indicated. (b) System setup for the playback process. A conjugate reference beam arrived at the PrC from the opposite direction and diffracted a conjugate beam toward the sample, retracing its path through the scattering material. The reconstructed beam was then focused to a spot and recorded at a CCD. A measurement of the phase conjugate power (OPC signal) was made at the location indicated.

## 2 Materials and Methods

The TSOPC system shown in Fig. 1 employs a 532-nm cw solid state laser in a Mach-Zehnder-type interferometry scheme. Light scattered on transmission through the sample (20-mW incident power, 2-mm collimated beam) interfered with a reference beam (10 mW), as depicted in Fig. 1(a). This interference pattern was written into a 45-deg cut iron-doped (0.015%) LiNbO<sub>3</sub> photorefractive crystal (PrC) over a time period of 20 s. The distance between the 10×20×20 mm crystal and the sample was set by the thickest sample used in each set of experiments. A phase conjugate reference beam (2 mW), approaching the PrC from the opposite direction, was used to play back the “time-reversed” wavefront, as seen in Fig. 1(b). The phase conjugate wavefront retraced its path through the sample, reconstructing the incident light field. The reconstructed collimated beam was focused by a lens ( $f = 10$  cm), and the TSOPC signal was then measured at a CCD camera over a variable integration time (0.25 ms to 1 s).

To reassure ourselves that we were achieving phase conjugation, we laterally displaced a representative tissue mimicking phantom over a range of 1.6  $\mu\text{m}$  while measuring the

reconstructed signal amplitude. This particular phantom was composed of 433-nm polystyrene spheres in polyacrylamide. It was 4.0 mm in thickness with a scattering coefficient of  $\mu_s=45.4 \text{ mm}^{-1}$  (strongly scattering compared to the phantoms used later in this manuscript). Since the “time reversal” process is dependent on the scatterers remaining in the same position during both recording and playback, we expect to see the signal fall off dramatically as the sample is displaced.

During the subsequent experiments, the sample remained stationary and several measurements were made. Direct transmission through the sample was measured over the collection area of the crystal ( $P_{T_{\text{meas}}}$ ). This was accomplished by aperturing the photodetector of a Newport power meter to the projected size of the reference beam in the PrC (approximately  $3.5 \times 10 \text{ mm}$ ). Additionally, we measured the power exiting the photorefractive crystal before returning to the sample ( $P_{\text{OPC}}$ ), and finally the TSOPC signal amplitude.

TSOPC measurements were made using two types of samples. The first were sections of chicken breast tissue ranging from 0.25 to 7 mm. The scattering coefficient of the tissue was measured interferometrically using a standard MachZehnder interferometer. When a slab of tissue was placed in the sample arm of the interferometer, only the ballistic component of the scattered light was capable of significantly interfering with the reference arm. The percent reduction in amplitude of the interference fringes between the case with a sample present and with a water-filled sample holder represented the ballistic transmission and was used to find the scattering coefficient from  $T_{\text{ballistic}}=\exp(-\mu_s L)$ .

We also performed measurements on tissue-mimicking phantoms composed of polystyrene microspheres embedded in polyacrylamide. The concentrations of microspheres were chosen to obtain scattering coefficients that varied between 0.1 and  $15 \text{ mm}^{-1}$  based on Mie theory calculations. The phantom samples were 3.5 mm in thickness. In addition to varying the scattering coefficient, the anisotropy factor was also varied by creating phantoms using four different sphere sizes (1003, 433, 157, and 80.9 nm diameter) corresponding to anisotropy factors of  $g=0.93, 0.83, 0.28,$  and  $0.07$ , respectively. The average sphere size was measured in a scanning electron microscope. The ballistic transmission through the phantoms was measured very far ( $\sim 6 \text{ m}$ ) from the sample, and the equation found in the preceding paragraph can again be used to determine the scattering coefficient. Only those samples whose measured scattering coefficient matched the intended scattering coefficient to within 10% were used for measurements.

For the preceding measurements, a collimated sample beam was incident on the scattering sample. Such measurements were repeated for resolution studies in a slightly modified scheme in which the sample beam (10 mW) was focused onto the front face of the scattering sample (as shown later in Fig. 6) using a 6.24-mm-focal-length lens. The scattered light pattern was written into the PrC upon interference with a reference beam (40 mW). In this manner, the reconstructed light field generated by a 1.5-mW conjugate reference beam, formed a spot that was then imaged onto the CCD camera with a magnification of  $\sim 69$  (given by the ratio of the focal lengths of the two lenses, where the lens in front of the CCD had a focal length of 43 cm). The PrC was placed 25 cm from

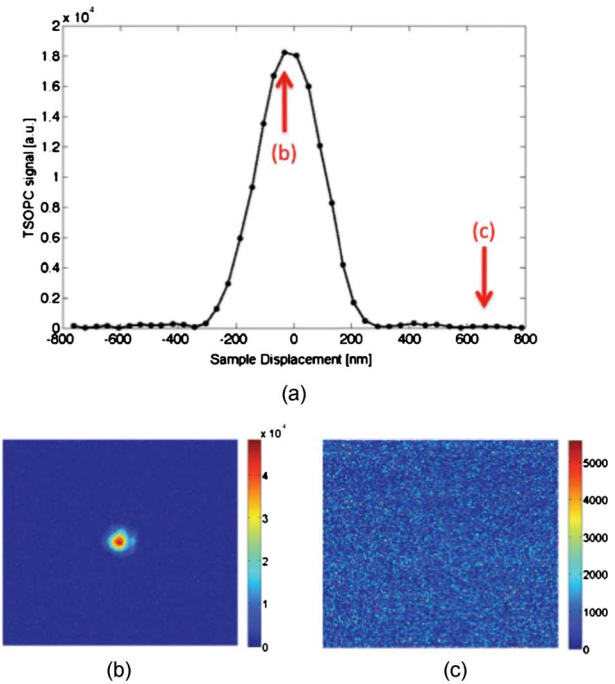


**Fig. 2** (a) Reconstructed TSOPC signal measured at the CCD as the sample is displaced over  $1.6 \mu\text{m}$ . (b) and (c) are images recorded at the locations indicated by the red arrows. This data confirms that we are measuring a phase conjugation signal that is dependent on the location of scatterers in the sample. (Color online only.)

the focused beam waist such that, in the absence of a scattering medium, the beam had diverged significantly (by a factor of  $\sim 4$ ) on reaching the reference beam (Fig. 5 in Sec. 3.3). The width of the measured spot, as determined through Gaussian fitting in two orthogonal directions, was then used to investigate the resolution of the TSOPC system.

### 3 Results

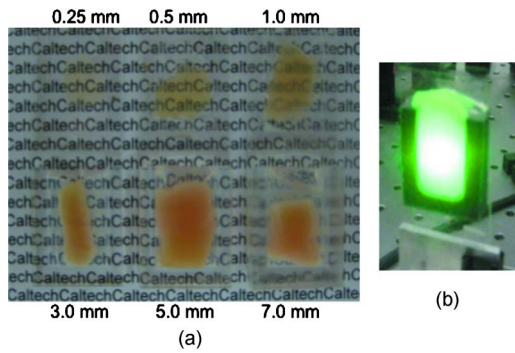
#### 3.1 Confirmation of Phase Conjugation

Figure 2 shows the decay of the signal measured at the CCD in Fig. 1 as a function of sample displacement. Notably, the reconstructed signal falls off dramatically as the sample is moved, implying that we are correctly performing the phase conjugation experiment. If we examine the images captured at displacements corresponding to the red arrows in Fig. 2(a), we see that the bright spot shown in Fig. 2(b) had completely disappeared and was buried in noise in Fig. 2(c). This serves as confirmation that we are seeing a phase conjugate signal that is dependent on the location of scatters in the sample.

#### 3.2 Chicken Breast Tissue Experiments

We first examine results from chicken tissue samples of varying thickness. Figure 3(a) shows representative samples indicating that the thickest tissue samples used in this study were by no means transparent. Figure 3(b) shows the large extent of light scattering experienced by a green incident beam ( $\lambda=532 \text{ nm}$ ).

We determined the scattering coefficient of the chicken breast tissue to be  $\mu_s=30.3 \text{ mm}^{-1}$ . The following data are reported as a function of the average number of scattering



**Fig. 3** (a) Representative 0.25-, 0.5-, 1-, 3-, 5-, and 7-mm-thick chicken breast sections placed above text. As the thickness increases, light scattering makes it impossible to read the text below. (b) A 3.5-mm-diam beam of 532-nm light scattering through a representative 7-mm section of chicken breast tissue. For reference, the black plastic spacer is  $30 \times 24$  mm.

events experienced by a photon tracing an approximately straight path through the sample, quantified by  $\mu_s L$  ( $L$  is the sample thickness). Although most photons take longer paths through the scattering material, scattering more than  $\mu_s L$  times, this is a simple reference quantity for turbidity estimation. In general the ballistic, or unscattered, component of the transmission decays exponentially with depth into a scattering medium,  $T_{\text{ball}} = \exp(-\mu_s L)$ . All data are normalized with respect to a nonscattering sample.

The total signal contained in the reconstructed focused spot, as measured on the CCD in Fig. 1(b), was indicative of the amount of light that had returned to its original configuration. For simplicity, this metric can be replaced by the amplitude, or peak intensity, of the focused spot, shown explicitly in Figs. 4(b) and 4(c). This is possible because the full width at half maximum (FWHM) of the reconstructed spot did not change as a function of scattering strength (a phenomenon that is discussed in detail later in this paper). The red curve in Fig. 4(a) displays the TSOPC amplitude as a function of  $\mu_s L$ . Error bars correspond to the standard error from measurements made over different sample locations (i.e., different random configurations of scatterers). Although the TSOPC amplitude initially dropped off quickly, the slope began to taper off more slowly as  $\mu_s L$  increased. This limited decrease is particularly noteworthy when compared to the dramatic decay of the ballistic component [blue curve, Fig. 4(a)].

The signals in Fig. 4(a) were measured in tissue sections that ranged from 0.25 to 7 mm in thickness, the thickest of which corresponding to a “time reversal” of more than 200 scattering events. This is by no means trivial. Transmission through the 7-mm tissue sample would result in a ballistic component at  $-91$  on the scale shown in Fig. 4(a), or an attenuation of  $-910$  dB.

The solid black curve in Fig. 4(a) represents the direct transmission through the chicken breast samples measured over the collection area of the PrC,  $T_{\text{meas}}$  [recorded at the location denoted in Fig. 1(a)]. The green curve shows a similar trend and represents the power that exited the PrC on playback, denoted  $P_{\text{OPC}}$  and recorded where indicated in Fig 1(b). The dependence of the TSOPC amplitude on these measured signals is discussed and modeled in Sec. 4.

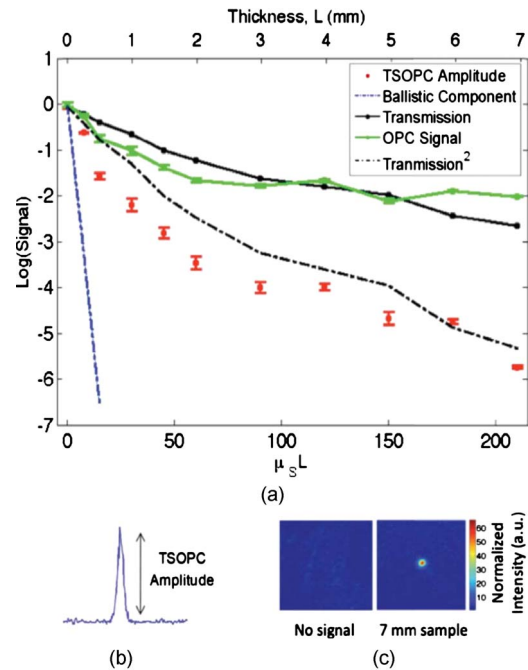


**Fig. 4** (a) TSOPC amplitude (red data), ballistic transmission (blue line), total transmission (black curve), and OPC signal (green curve) as levels of scattering were increased. The square of the transmission (dashed curve) approximated the TSOPC amplitude in trend. Error bars represent the standard error over  $N$  ranging from three to seven measurements. (b) TSOPC amplitude was measured as the height of the focused spot after the background signal was subtracted. (c) Signal from the 7-mm chicken breast sample was clearly visible above the noise in the system. (Color online only.)

### 3.3 Tissue-Mimicking Phantom Experiments

To examine the dependence of our system on the angular scattering properties of the sample, we conducted experiments on tissue-mimicking phantoms composed of polystyrene spheres embedded in polyacrylamide. By varying the size of the spheres, the anisotropy factor,  $g$ , of the scattering media can be altered. A measure of the angular spread of the scattered light  $g$  is defined as the average cosine of the scattering angle [ $g = \langle \cos(\theta) \rangle$ ]. Figure 5(a) shows the TSOPC amplitude as a function of  $\mu_s L$  for four types of phantoms from highly forward scattering ( $g=0.93$ ) to nearly isotropic ( $g=0.07$ ). We found that the more forward scattering samples resulted in a larger TSOPC signal for the same  $\mu_s L$ . The solid line superimposed on the data in Fig. 5(a) shows the decay of the ballistic component of the transmission, while the dashed line shows the decay of the ballistic component through a sample twice as thick ( $2L$ ). Except for the case of the highly forward scattering samples, the TSOPC amplitude initially decayed along the dashed line.

### 3.4 Resolution Trends

To study the resolution of our TSOPC experiment, we employed a modified system in which the sample beam was focused onto the front face of the sample [Fig. 6(a)]. The remainder of the system is as described in Fig. 1, and phase conjugation was used to reconstruct this spot at the front face of the sample. An imaging system formed between the lens

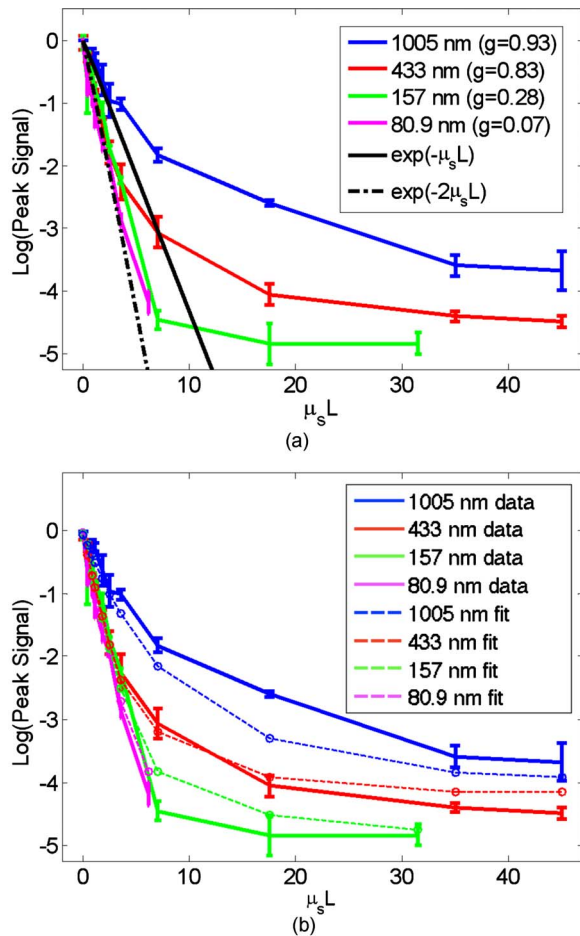


**Fig. 5** TSOPC amplitude trend for tissue-mimicking phantoms composed of polyacrylamide ( $n=1.346$ ) with embedded polystyrene microspheres ( $n=1.6$ ). (a) The amplitude signals fell off more dramatically for smaller spheres with a lower anisotropy factor. The black curve represents the ballistic transmission through the samples, and the dashed curve represents the ballistic transmission through a sample twice as thick. (b) The TSOPC amplitude curves compared to the square of the transmission, showing that they agree in trend for the various sphere sizes.

shown in Fig. 6(a) and that in front of the CCD in Fig. 1(b) was used to relay and magnify the reconstructed spot onto the camera for detection. The spot sizes described in the following results refer to the spot size at the sample.

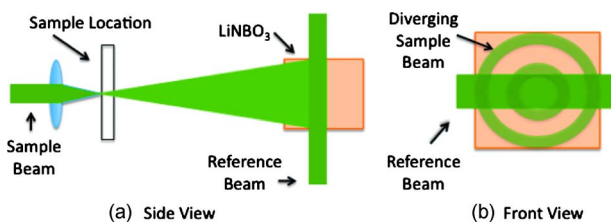


**Fig. 6** With no sample present, the light diverging from a focused beam expands on its path to the photorefractive crystal. Using a reference beam of fixed width, angular components of the diverging beam are better captured along one axis: (a) side view and (b) front view.

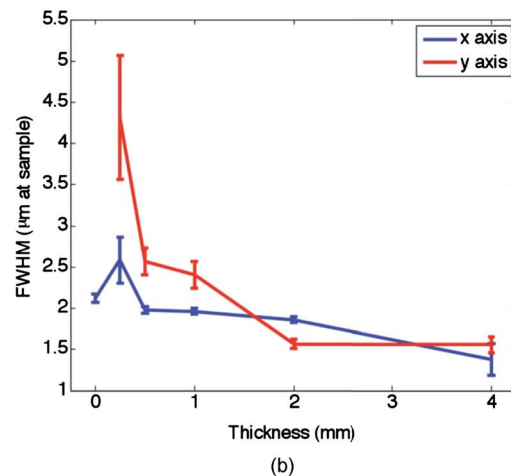
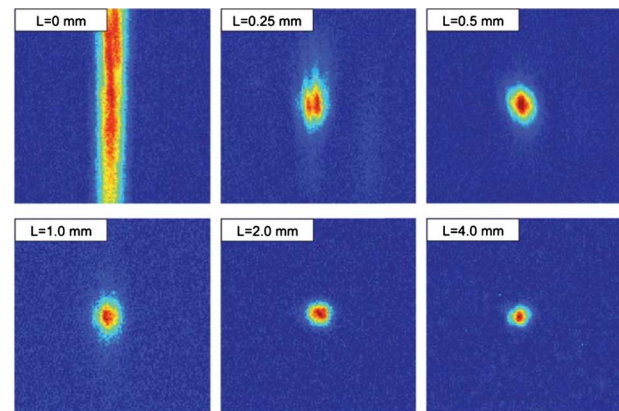


**Fig. 7** Chicken tissue samples. (a) The top left panel shows that with no sample present the reconstructed signal forms a stripe rather than a spot. The other panels show that as the scattering is increased, the stripe is reduced to a near diffraction limited spot. (b) The reduction in the size of the focused spot in the  $x$  and  $y$  directions. The diffraction limit in this setup was calculated to be  $1.2 \mu\text{m}$ . Error bars represent the standard error of the FWHM made over  $N=3$  measurements.

We found that with no scattering sample present, the measured spot was narrow in the horizontal dimension, but spread over a large range vertically [top left panel of Fig. 7(a)]. However, this effect could be mitigated through the presence of strong scattering in the sample. Figure 7(b) shows the FWHM of the reconstructed spot in both the  $x$  and  $y$  directions for increasing thicknesses of chicken breast samples. Both values tapered to tight ( $\sim 1.5 \mu\text{m}$ ), nearly diffraction limited (calculated to be  $1.2 \mu\text{m}$ ) spots, although the FWHM in the  $x$  direction tapered more quickly. The same trend can be seen with tissue-mimicking phantoms in Fig. 8.

## 4 Discussion

### 4.1 Amplitude Trends in Tissue Samples

To understand the TSOPC amplitude trend, we observed the corresponding trends for other measurable quantities in the system, including the transmission and OPC signals plotted in Fig. 4(a). As the thickness of the chicken sections were increased, both the transmission and OPC signal decayed in a similar manner. This shows that the power exiting the PrC

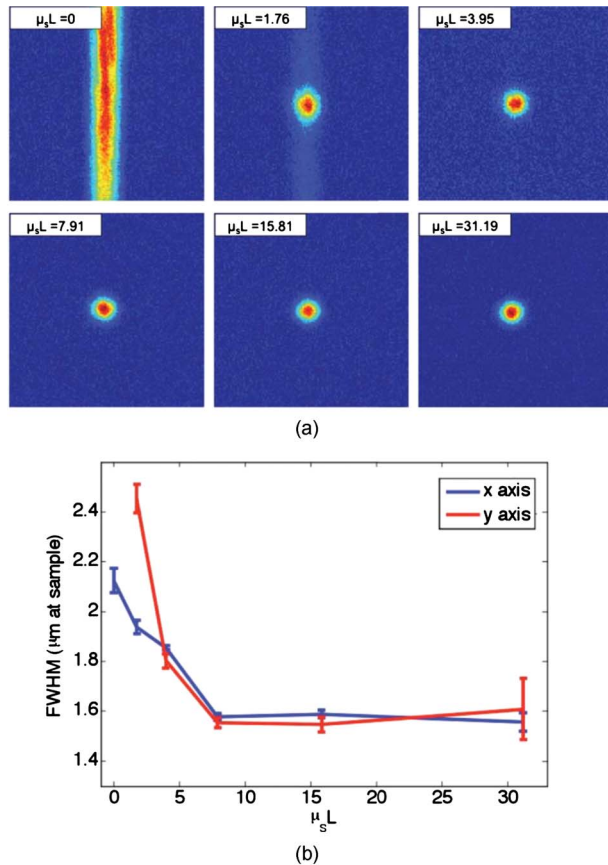


**Fig. 8** Tissue-mimicking phantoms. (a) The top left panel shows that with no sample present the reconstructed signal forms a stripe rather than a spot. The other panels show that as the scattering is increased, the stripe is reduced to a near diffraction limited spot. (b) The reduction in the size of the focused spot in the  $x$  and  $y$  directions. The diffraction limit in this setup was calculated to be  $1.2 \mu\text{m}$ . Error bars represent the standard error of the FWHM made over  $N=3$  measurements.

playback is proportional to the sample power entering the crystal during the recording process. Although we saw the transmission and OPC signals fall off in a similar manner, we saw a large discrepancy between these and the TSOPC amplitude (red curve). The origins of this trend will be discussed and modeled later in this section.

The signal we measured through the thickest chicken tissue sample requires additional discussion. One might expect that efficient “time reversal” would be dependent on the collection of the entire scattered wavefront. However, a measurement of the total transmission through a 7-mm chicken breast sample over the collection area of the PrC shows that only  $\sim 0.02\%$  of the power incident on the sample is scattered into the collection region. This implies that at most  $0.02\%$  of the incident power is used to record the hologram for phase conjugation, and is important because it shows that the TSOPC process is capable of “time reversal” even when only a small portion of the scattered wavefront is captured. The 7-mm thickness of chicken breast tissue does not represent a hard limitation on the capabilities of our system. It was simply the thickest sample that we measured in this study.

To cast our results in a slightly different light, consider an OCT system centered at 532 nm with 120 dB of SNR. If we tried to image these chicken samples with such a system, we would find that our depth penetration is limited by scattering to  $\sim 0.5$  mm, or  $\mu_s L \sim 15$ . Although we are not imaging, our measured TSOPC signal through 7 mm of highly scattering tissues is noteworthy in the context of current biomedical imaging standards.

#### 4.2 Amplitude Trends in Tissue-Mimicking Phantoms

The amplitude signals recorded using tissues phantoms were shown to depend on the  $g$  factor of the sample. This is due to the limited collection angle of the PrC. Forward scattering events were more likely to direct a photon toward the PrC, while isotropic scattering events were likely to direct a photon away from it. Thus, the final measured signal for isotropically scattering samples was less than that for forward scattering samples.

It is interesting that the measured signals in Fig. 5(a) fall off along the dashed line, corresponding to the ballistic component of light transmitted through a sample of double thickness. A measured TSOPC amplitude close to the dashed line implies that no advantage is gained by performing the TSOPC experiment. However, as  $\mu_s L$  increased, the TSOPC amplitude began to diverge from the dashed line, meaning that we started to see an increased signal through TSOPC. The ballistic component of the scattered light was initially much stronger than the TSOPC signal, which became visible only after the ballistic component decayed significantly. In sum, Fig. 5(a) shows that we can efficiently collect forward scattered light, and implies that the majority of the signal we measure in tissues is related to forward directed scattering events as opposed to isotropically directed scattering events.

#### 4.3 Origins of Amplitude Trends

A simple predictor of the TSOPC amplitude is square of  $T_{\text{meas}}$ , shown as a dashed black curve in Fig. 4(a) and dashed curves in Fig. 5(b). This finding is in agreement with literature results in which phase conjugation was studied.<sup>11,12</sup> Gu and Yeh<sup>11</sup> invoked the reciprocity theorem and conservation of energy to show that under ideal circumstances (specifically in the absence of absorption and backscattering), the fidelity of the process, equivalent to our amplitude measure, scales as the square of the fraction of light intercepted by the phase conjugating device. This was experimentally verified using scattering sheets of polypropylene and polyethylene.<sup>12</sup> Our samples are by no means ideal, most notably in terms of non-negligible absorption and backscattering of the tissue samples. The agreement of our TSOPC amplitude (red curve) with the square of the transmission (dashed black curve), at least in terms of trend, confirms that these predictions hold true for the case of tissue scattering as well. Our results serve to validate this theoretical prediction for a broader range of applications.

This finding deserves additional discussion. We can describe the total “time-reversed” transmission as the product of the power leaving the PrC and the transmission of the phase conjugated beam:  $P_{\text{TSOPC}} = T_{\text{OPC}} P_{\text{OPC}}$ . One may argue that if each photon trajectory is perfectly phase conjugated and efficiently “time reversed,”  $T_{\text{OPC}}$  would trend toward a value of

1, and all power directed into the sample would be effectively transmitted. The flaw in this argument is that fundamentally, our experiment cannot be described by a photon picture. If we think of the sample as a black box, and monitor only the fraction of the input light that exits one side of the box, we can make an interesting comparison. If the box contains a 50/50 beamsplitter (BS), we would expect 50% of the input power to exit. If we phase conjugated the exiting light, we would expect a second decrease of 50% on the way back. Although this may appear to be a very different scenario, in reality it is quite similar. In our TSOPC experiment, we can think of dividing the scattered wave into groups that have passed through channels with a particular transmission coefficient (as in Ref. 10). The bulk of the incident light is diffusely reflected, so the majority of the channels possess very small transmission coefficients. However, a small set of these channels transmits light in a fairly efficient manner. Each of these channels can be likened to a BS with a fixed transmission coefficient. When the light is phase conjugated back along these paths, they again transmit the same fraction of light. Thus, in reality, the  $T_{\text{OPC}}$  is equivalent to the transmission of an incident plane wave through the sample.

In our current setup, where  $P_{\text{OPC}}$  scales with  $T_{\text{meas}}$ , the preceding argument confirms the  $T_{\text{meas}}^2$  dependence predicted by Gu and Yeh. The amplitude of the transmitted light is the same as that expected by a double pass through the sample. The advantage, however, is that instead of the diffuse transmission that would result if a conventional mirror was used to reflect light back through the sample, we see the phase conjugate beam regain spatial coherence to reconstruct the incident light field. If a digital version of this experiment was employed, by recording the interference of the scattered field with a reference beam on a camera and playing back the phase conjugate field with a spatial light modulator, then  $P_{\text{OPC}}$  could be increased arbitrarily and enhanced transmission may be possible.

Although the  $T_{\text{meas}}^2$  curves agree with our data in trend, they do not provide a very close fit, especially for the tissue-mimicking phantom results. Although the properties of the sample are accounted for, the properties of the phase conjugation are not. In the Appendix, we formulate a model that includes both  $T_{\text{meas}}$  and  $P_{\text{OPC}}$  values to describe the crossover from ballistic to diffusive regimes. The result is as follows:

$$\frac{P_{\text{TSOPC}}}{P_{\text{norm}}} = \left\{ T_{\text{ball}} + X \left( \frac{P_{\text{OPC}}}{P_{\text{norm}}} - T_{\text{ball}} \right) (T_{\text{meas}} - T_{\text{ball}}) \right\}^{1/2} \quad (1)$$

where  $P_{\text{norm}}$  is the measured OPC power with no sample present. If we make the assumption that the aperture of the PrC is sharp,  $X^2$  represents the ratio of the active area/responsivity of the PrC to the active area/responsivity of the photodetector used to measure the transmission. This assumption is not valid in reality since the aperture of the PrC is determined by the size of the Gaussian reference beam (not sharp). However, the trend of the  $X^2$  values is still illuminating.

Figure 9 shows fits of this model to both the tissue [Fig. 9(a)] and phantom data [Fig. 9(b)]. The fits are significantly better than the  $T_{\text{meas}}^2$  fits for all types of samples since infor-

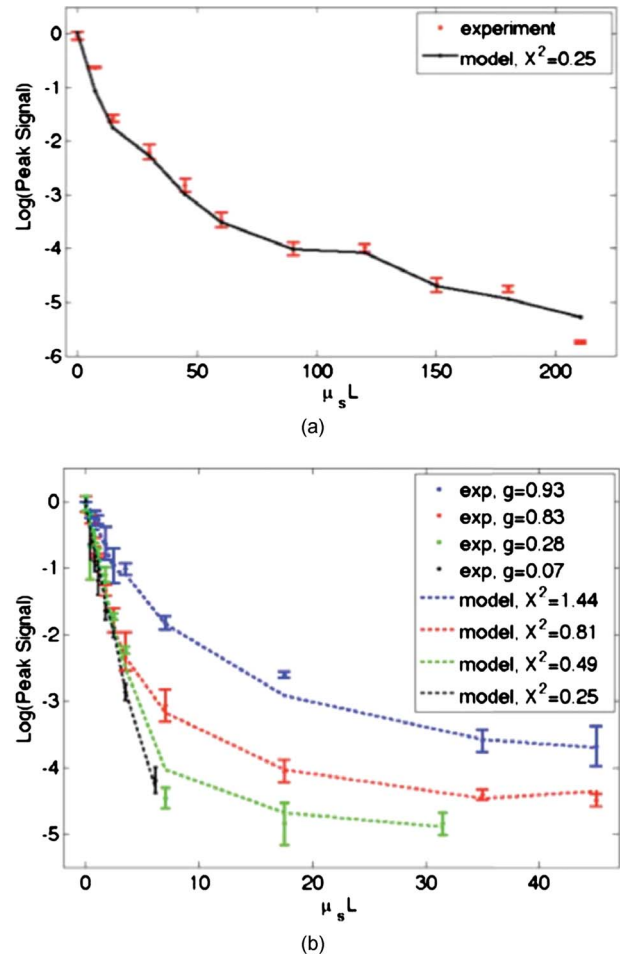


**Fig. 9** Model fits to (a) the experimental chicken tissue results and (b) the experimental tissues phantom results. A model that includes information about both the sample and the phase conjugation performs significantly better than the  $T^2$  predictor in both cases.

mation about both the sample and the phase conjugation are taken into account. If we examine the  $X^2$  values from fits to the phantom data [Fig. 9(b)], we see that  $X^2$  decreases with the anisotropy factor  $g$ . This is attributable to the fact that the responsivity of the PrC is diminished when scattered light enters the active area at increasing angles with respect to the incident beam. This serves to reduce the amplitude of the interference pattern written into the PrC, and results in the same outcome as the case of a PrC with optimal responsivity that shrinks in size as the  $g$  factor decreases. Since tissues are highly forward scattering, we might expect that a fit to the chicken tissues sections would result in an  $X^2$  similar to that of the 1- $\mu\text{m}$  beads. However, we found a much smaller  $X^2$  value. We expect that this occurred because the chicken sections are nonideal scattering samples. The speckle pattern formed by the scattered light is not stationary due to diffusion of particles within the tissues. This implies that the particular channels that existed throughout the recording process do not necessarily exist or possess the same transmission coefficient on playback. Thus, even if a strong pattern is formed at the PrC, it may not exactly correspond to the scattering structure of the tissue on playback. A faster holographic medium or a

digital implementation of this experiment may diminish this effect in the future.

#### 4.4 Resolution Trends

One might expect that the resolution of the TSOPC system would degrade as scattering becomes more prominent. However, we found that scattering can be beneficial in terms of resolution when a limited collection angle is employed. This experiment represented a low collection efficiency situation because the PrC was placed far from the sample plane. With no scattering sample in place, Fig. 6(a) shows that the sample beam had diverged significantly on reaching the PrC, and only portions of the sample beam that overlapped with the reference beam were recorded. From a Fourier optics perspective, the large-angle components of the diverging beam carried information about high spatial frequencies at the focus. Thus, by losing these components, we could no longer expect to reconstruct a diffraction-limited spot. As the sample and reference beams were orthogonally oriented in the crystal [Fig. 6(b)], the effective recording area for the sample beam had a width of 3.5 mm (FWHM of the collimated reference beam) and length of 10.0 mm (length of the crystal). This explains the shape of the spots shown in Figs 7(a) and 8(a). Since the collection region was oblong, diverging angular components were better captured along one axis, leading to a smaller reconstructed spot along that dimension. As the samples became more highly scattering, more of the angular components were directed into the PrC, and the spot size was improved. The tapering of the FWHM to a constant value implies that beyond a scattering threshold, the angular components incident on the sample were effectively randomized such that efficient collection could be obtained over any small portion of the scattered wavefront. This finding was demonstrated previously for plastic sheet aberrators and etched glass phase screens,<sup>13</sup> confirming theory and simulations on thin, random phase screen aberrators,<sup>14,15</sup> but has never been demonstrated in extended scattering samples or biological materials. Our work serves to extend these findings into the realm of realistic biological materials.

We mentioned previously in discussing our amplitude results that the peak of the detected signal was a useful metric only if the width of the spot remained constant. There were two significant differences in system geometry between the amplitude experiments and the resolution experiments described immediately above. First, the sample beam was collimated as opposed to focused on the sample. This reduced the beam divergence toward the crystal. Second, the PrC was placed as close as possible to the sample plane. Both of these geometrical factors allowed for efficient collection regardless of the level of scattering. Thus, throughout the amplitude experiments described, the FWHM of the measured spot was fixed for all measurements. Our amplitude studies showed that we could reconstruct a signal with only a small portion of the scattered wavefront, and our resolution studies provided us with evidence to claim that all relevant information was contained in this reconstruction.

#### 4.5 Significance and Future Work

Note that our results, in both tissues and tissue-mimicking phantoms, contrast the common misconception that light loses

its coherence on scattering. While a tight pulse of light spreads as scattering occurs and spatial coherence is certainly lost, individual portions of the wavefront traveling on various trajectories through the scattering media retain relative coherence and thus are still capable of interference. We have shown a signal, dependent on coherent recording and playback mechanisms, for light that has scattered over 200 times on average. However, polarization shifts can accrue during scattering and, in the case where the scattered light is sufficiently diffuse, the light field no longer possesses a preferred polarization state. As light of an orthogonal polarization cannot interfere with the reference beam, we can expect to record at most half of the available information in this situation. We believe that future technological developments of TSOPC systems should include the capability for recording the scattered wavefront using two orthogonal polarizations, demonstrated to be useful in a related system in Ref. 10.

Although the current implementation of TSOPC has not yet been applied for imaging, diagnostics, or therapy, we envision several potentially useful applications of our technique. In the context of photodynamic therapy (PDT), it may be possible to conjugate PDT agents to strong scatterers, which can then be injected into a region to be ablated. The collected scattered light field will encode the locations of these strong scatterers, and playback (with an OPC field of increased optical power) will direct large amounts of light to the scatterer/PDT agent construct. This type of experiment would enable a clinician to target light delivery to injected agents while avoiding the remainder of the sample. Additionally, an iterative implementation of the experiment could be useful for highlighting weak absorbers buried in a scattering medium. Elastic scattering would be “time reversed” on each iteration, but absorption would occur during each pass. This could potentially enable sensitive measurements of absorbers such as glucose through a noninvasive measurement. Ideally, beyond these applications, the long-term goal of this line of research is to facilitate high-resolution deep tissue imaging.

## 5 Conclusions

We demonstrated that we can efficiently suppress elastic light scattering in tissues and tissue-mimicking phantoms using optical phase conjugation. We examined the decay of the reconstructed TSOPC amplitude as a function of  $\mu_s L$  and found that, after an initial sharp drop, the signal decreased slowly compared to the decrease in ballistic transmission. This amplitude trend roughly scaled as the square of the transmission through the samples, and was modeled more accurately using measurements that included both sample and phase conjugation effects. TSOPC signals were measured through up to 7 mm of chicken breast tissue, displaying effective reconstruction through coherent mechanisms after an average of over 200 scattering events. Additionally, we showed that as little as 0.02% of the scattered wavefront was sufficient for a TSOPC reconstruction. Measurements on tissue-mimicking phantoms confirmed the amplitude trends, and showed that more highly forward scattering samples led to larger TSOPC amplitude values as more scattered components were directed into the collection region of the PrC. Finally, increased scattering in both tissues and tissue mimicking phantoms was found to improve the resolution of the detected signals by



improving the overall angular collection efficiency of the system.

## Appendix

We consider the situation in which a phase conjugate mirror (PCM) is placed behind a scattering medium. The PCM can be any phase-conjugating device including the holographic setup employing a PrC described in this manuscript. Light that propagates through the medium is phase conjugated and retraces its path back through the scattering medium to refocus at its origin. This section describes the trend of the intensity of the refocused light, for samples ranging from thin (transmission is mostly ballistic) to optically thick (transmitted light is completely diffuse). We assume that light propagation in the medium is reciprocal and that there are no nonlinear effects. We make no assumptions about absorption, the efficiency of the PCM, light propagation, etc. unless explicitly stated.

Following the conventions of Gu and Yeh,<sup>11</sup> we define the incident field  $E_1$ , the transmitted field  $E_2$ , the phase-conjugated field  $E_3$ , and the field that has been transmitted back through the sample  $E_4$ . Scattering in the sample is described by the scattering function  $h$  such that

$$E_2(x',y') = \iint E_1(x,y)h(x,y,x',y')dx dy, \quad (2)$$

with input coordinates  $(x,y)$  and output coordinates  $(x',y')$ . Because of reciprocity, propagation back is described by

$$E_4(x,y) = \iint E_3(x',y')h(x,y,x',y')dx' dy'. \quad (3)$$

For simplicity, we take the incident field to be a delta function<sup>†</sup> with amplitude  $E_{\text{in}} \equiv \sqrt{P_{\text{in}}}$ , where  $P_{\text{in}}$  is the total incident power.

The fields propagating toward the PCM are now given by

$$E_1(x,y) = E_{\text{in}}\delta(x,y), \quad (4)$$

$$E_2(x',y') = E_{\text{in}}h(0,0,x',y'). \quad (5)$$

At the PCM, the field is reflected and phase conjugated. Since the PCM is not perfect, the reflected field has a certain envelope  $\alpha\rho(x',y')$ , where  $\rho(0,0)=1$ , and  $\alpha$  is the overall reflection coefficient of the phase conjugation.<sup>‡</sup> If the PCM reflects the field with exactly the same amplitude,  $\alpha=1$ ,

$$E_3(x',y') = \alpha\rho(x',y')E_2^*(x',y'). \quad (6)$$

For the reconstructed field  $E_4$ , we are interested only in the part that overlaps with the incident field. The total power in this overlapping portion is given by

<sup>†</sup>In reality the incident field will not be a delta function. Regardless of the actual shape of the incident field, we are free to choose a coordinate system where the incident field corresponds to a delta function by applying an arbitrary unitary transform. Therefore, the results derived here are generally valid.

<sup>‡</sup>In practice,  $\alpha$  is not exactly constant over different experiments due to a number of reasons including the nonuniformity of the PCM, power fluctuations of the laser, and experimental human error from run to run. These fluctuations are visible in the data shown in this manuscript.

$$P_{\text{TSOPC}} \equiv \iint \delta(x,y)|E_4(x,y)|^2 dx dy = |E_4(0,0)|^2, \quad (7)$$

with

$$E_4(0,0) \equiv \alpha E_{\text{in}} \iint \rho(x',y')|h(0,0,x',y')|^2 dx' dy', \quad (8)$$

where Eqs. (3), (5), and (6) were used.

Two other important quantities in the experiment are the total transmitted power  $P_T$  (or  $P_2$ ), and the total power exiting the PCM  $P_{\text{OPC}}$  (or  $P_3$ ). These can be described as follows:

$$\begin{aligned} P_T &= \iint |E_2(x',y')|^2 dx' dy' \\ &= P_{\text{in}} \iint |h(0,0,x',y')|^2 dx' dy' = P_{\text{in}}T, \end{aligned} \quad (9)$$

where  $T$  is the total (angle integrated) transmission. To simplify this notation we define

$$|h(0,0,x',y')|^2 \equiv TF(x',y'), \quad (10)$$

where  $F$  is the intensity profile of the transmitted light, normalized such that  $\iint F(x',y')dx' dy' = 1$ . Using this notation, the power exiting the PCM is given by

$$\begin{aligned} P_{\text{OPC}} &= \iint |E_3(x',y')|^2 dx' dy' \\ &= \alpha^2 P_{\text{in}} \iint \rho^2(x',y')|h(0,0,x',y')|^2 dx' dy' \\ &= \alpha^2 P_{\text{in}}TC_3, \end{aligned} \quad (11)$$

where

$$C_3 \equiv \iint \rho^2(x',y')F(x',y')dx' dy'. \quad (12)$$

Here,  $C_3$  describes the fraction of light that is “seen” by the PCM. In Gu and Yeh,  $C_3$  is approximated as  $a/A$ , where  $a$  is the surface area of the PCM, and  $A$  is the total surface area of the diffuse light.

Using the same notation, Eq. (7) can be rewritten as

$$P_{\text{TSOPC}} = \alpha^2 P_{\text{in}}T^2C_4^2, \quad (13)$$

where

$$C_4 \equiv \iint \rho(x',y')F(x',y')dx' dy'. \quad (14)$$

Note that  $C_3 \neq C_4$ ;  $C_3$  describes the fraction of the intensity that is reflected, while  $C_4$  can be thought of as the fraction of the amplitude. In the special case described by Gu and Yeh, which includes a sharp aperture and uniform phase conjugation (i.e.,  $\rho=1$  or  $\rho=0$ ),  $C_3=C_4$ . In general, however, they are different.

We can now predict the trend of the TSOPC power by combining Eqs. (12) and (14):

$$P_{\text{TSOPC}} = P_{\text{OPC}} T \frac{C_4}{C_3}. \quad (15)$$

The difficulty with this form is that a measurement of the total transmission  $T$  is very hard. In our experiments, the transmission is measured over a defined aperture associated with the photodetector, chosen to be approximately the same shape as the reference beam in the photorefractive crystal. The transmission measured in this manner  $T_{\text{meas}}$  is related to the total transmission  $T$  according to

$$T_{\text{meas}} = \frac{1}{P_{\text{in}}} \iint \rho_{\text{meas}}^2(x', y') |E_2(x', y')|^2 dx' dy' = TC_2, \quad (16)$$

where  $\rho_{\text{meas}}^2$  is the (intensity) profile of the aperture over which the transmission is measured, and

$$C_2 = \iint \rho_{\text{meas}}^2(x', y') F(x', y') dx' dy'. \quad (17)$$

Finally, we can write the TSOPC amplitude trend as a function of the measured values  $T_{\text{meas}}$  and  $P_{\text{OPC}}$ .

$$P_{\text{TSOPC}} = P_{\text{OPC}} T_{\text{meas}} \frac{C_4}{C_2 C_3}. \quad (18)$$

The constant  $C_4/C_2 C_3$  must be determined experimentally.

In the diffuse regime, we can use Eq. (18) to predict the trend of the TSOPC amplitude. However, when the samples are so thin that the ballistic contribution becomes visible, the distribution of the transmitted intensity  $F$  will be different than in the diffuse case. As a result, the preceding constants will depend on the thickness of the samples. To deal with this complication, we introduce a simple model. We assume that there are only two contributions to the transmission: completely ballistic and completely diffuse. Thus, we can write

$$TF(x', y') = T_{\text{ball}} \delta(x', y') + T_{\text{diff}} F_{\text{diff}}(x', y'), \quad (19)$$

where  $F_{\text{diff}}(x', y')$  is the normalized profile of the diffuse transmission:  $\iint F_{\text{diff}}(x', y') dx' dy' \equiv 1$ . For thick samples,  $F \rightarrow F_{\text{diff}}$ . The Beer-Lambert law gives us the transmission coefficient for the ballistic component, and the transmission for the diffusive component follows from our earlier assumptions:

$$T_{\text{ball}} = \exp(-\mu_s L), \quad (20)$$

$$T_{\text{diff}} = T - T_{\text{ball}}. \quad (21)$$

Through this model, the total transmission remains equal to  $T$ . The values for  $C_2$ ,  $C_3$ , and  $C_4$  follow by inserting the model [Eqs.(19)] into their respective definitions:

$$TC_2 = T_{\text{ball}} + T_{\text{diff}} C_2', \quad (22)$$

$$TC_3 = T_{\text{ball}} + T_{\text{diff}} C_3', \quad (23)$$

$$TC_4 = T_{\text{ball}} + T_{\text{diff}} C_4', \quad (24)$$

where the ballistic component is always completely detected/reflected since  $\rho(0,0) = \rho_{\text{meas}}(0,0) = 1$ . The constant  $C_2'$  is defined as

$$C_2' = \iint \rho_{\text{meas}}^2(x', y') F_{\text{diff}}(x', y') dx' dy', \quad (25)$$

analogous to Eq. (17), and similarly for  $C_3'$  and  $C_4'$ . These constants are calculated for only the diffuse portion of the distribution and therefore do not depend on the sample thickness.

To predict the trend of the TSOPC power, we use the following procedure to process the measurements. First, we take the measured OPC power ( $P_{\text{OPC}}$ ),

$$P_{\text{OPC}} = P_{\text{in}} \alpha^2 (T_{\text{ball}} + T_{\text{diff}} C_3'), \quad (26)$$

and normalize it by the OPC power when no sample is present ( $P_{\text{norm}} = P_{\text{in}} \alpha_0^2$ ), where  $\alpha_0$  is the value of  $\alpha$  for the first measurement in the series (i.e., no sample). We then subtract the ballistic transmission to arrive at

$$\frac{P_{\text{OPC}}}{P_{\text{norm}}} - T_{\text{ball}} = \left( \frac{\alpha^2}{\alpha_0^2} - 1 \right) T_{\text{ball}} + \frac{\alpha^2}{\alpha_0^2} T_{\text{diff}} C_3' \approx \frac{\alpha^2}{\alpha_0^2} T_{\text{diff}} C_3'. \quad (27)$$

We must assume here that  $\alpha$  does not fluctuate too wildly ( $\alpha \approx \alpha_0$ ) so that the ballistic component can be removed. We do the same for the measured transmission  $T_{\text{meas}}$  (no normalization required):

$$T_{\text{meas}} - T_{\text{ball}} = T_{\text{diff}} C_2'. \quad (28)$$

We now multiply Eqs. (27) and (28) before taking the square root such that the resulting value scales linearly with  $\alpha$  and  $T_{\text{diff}}$ :

$$\left[ \left( \frac{P_{\text{OPC}}}{P_{\text{norm}}} - T_{\text{ball}} \right) (T_{\text{meas}} - T_{\text{ball}}) \right]^{1/2} = \frac{\alpha}{\alpha_0} T_{\text{diff}} (C_2' C_3')^{1/2}. \quad (29)$$

Our equation for the TSOPC power reads as follows after substituting Eq. (24) into Eq. (13):

$$P_{\text{TSOPC}} = P_{\text{in}} \alpha^2 (T_{\text{ball}} + T_{\text{diff}} C_4')^2. \quad (30)$$

We can determine this value by multiplying Eq. (29) by  $X \equiv C_4' / (C_2' C_3')^{1/2}$ , adding  $T_{\text{ball}}$ , and taking the square:

$$\begin{aligned} & \left\{ T_{\text{ball}} + X \left[ \left( \frac{P_{\text{OPC}}}{P_{\text{norm}}} - T_{\text{ball}} \right) (T_{\text{meas}} - T_{\text{ball}}) \right]^{1/2} \right\}^2 \\ &= \left( T_{\text{ball}} + \frac{\alpha}{\alpha_0} T_{\text{diff}} C_4' \right)^2 \approx (T_{\text{ball}} + T_{\text{diff}} C_4')^2 = \frac{P_{\text{TSOPC}}}{\alpha^2 P_{\text{in}}} \\ &= \frac{P_{\text{TSOPC}}}{P_{\text{norm}}}. \end{aligned} \quad (31)$$

The left-hand side of this equation is fit to the data in the manuscript, and the value of  $X$  is fit. The value  $X$  scales the contribution of the diffuse light based on the various aperture functions described in this derivation. If the aperture of the PCM is sharp, then  $C'_3$  and  $C'_4$  are equal. In this case,  $X^2$  is the ratio of the active area of the PCM to the active area of the photodetector.

### Acknowledgements

The authors gratefully acknowledge Christopher Kovalchick and Guruswami Ravichandran for sharing their expertise on polyacrylamide. The authors also thank Shuo Pang for making scanning electron microscope (SEM) particle size measurements. This work was supported by a National Science Foundation (NSF) Career Award, Grant No. BES-0547657, as well as National Institutes of Health (NIH) Grant No. R21 EB008866-01. E. McDowell acknowledges support from a NSF graduate research fellowship.

### References

1. Z. Yaqoob, D. Psaltis, M. S. Feld, and C. Yang, "Optical phase conjugation for turbidity suppression in biological samples," *Nature Photon.* **2**(2), 110–115 (2008).
2. E. N. Leith and J. Upatniek, "Holographic imagery through diffusing media," *J. Opt. Soc. Am.* **56**(4), 523 (1966).
3. M. D. Levenson, "High-resolution imaging by wave-front conjugation," *Opt. Lett.* **5**(5), 182–184 (1980).
4. M. C. Gower, "KrF laser-amplifier with phase-conjugate Brillouin retroreflectors," *Opt. Lett.* **7**(9), 423–425 (1982).
5. I. V. Tomov, R. Fedosejevs, D. C. D. Mcken, C. Domier, and A. A. Offenberger, "Phase conjugation and pulse-compression of KrF-laser radiation by stimulated Raman-scattering," *Opt. Lett.* **8**(1), 9–11 (1983).
6. D. Huang, E. A. Swanson, C. P. Lin, J. S. Schuman, W. G. Stinson, W. Chang, M. R. Hee, T. Flotte, K. Gregory, C. A. Puliafito, and J. G. Fujimoto, "Optical coherence tomography," *Science* **254**(5035), 1178–1181 (1991).
7. A. P. Gibson, J. C. Hebden, and S. R. Arridge, "Recent advances in diffuse optical imaging," *Phys. Med. Biol.* **50**(4), R1–R43 (2005).
8. D. A. Boas, D. H. Brooks, E. L. Miller, C. A. DiMarzio, M. Kilmer, R. J. Gaudette, and Q. Zhang, "Imaging the body with diffuse optical tomography," *IEEE Signal Process. Mag.* **18**(6), 57–75 (2001).
9. I. M. Vellekoop and A. P. Mosk, "Focusing coherent light through opaque strongly scattering media," *Opt. Lett.* **32**(16), 2309–2311 (2007).
10. I. M. Vellekoop and A. P. Mosk, "Universal optimal transmission of light through disordered materials," *Phys. Rev. Lett.* **101**(12), 120601 (2008).
11. C. Gu and P. C. Yeh, "Partial phase conjugation, fidelity, and reciprocity," *Opt. Commun.* **107**(5–6), 353–357 (1994).
12. I. McMichael, M. D. Ewbank, and F. Vachss, "Efficiency of phase-conjugation for highly scattered light," *Opt. Commun.* **119**(1–2), 13–16 (1995).
13. D. C. Jones and K. D. Ridley, "Experimental investigation by stimulated Brillouin scattering of incomplete phase conjugation," *J. Opt. Soc. Am. B* **14**(10), 2657–2663 (1997).
14. E. Jakeman and K. D. Ridley, "Incomplete phase conjugation through a random-phase screen. 1. Theory," *J. Opt. Soc. Am. A Opt. Image Sci. Vis* **13**(11), 2279–2287 (1996).
15. K. D. Ridley and E. Jakeman, "Incomplete phase conjugation through a random phase screen. 2. Numerical simulations," *J. Opt. Soc. Am. A Opt. Image Sci. Vis* **13**(12), 2393–2402 (1996).